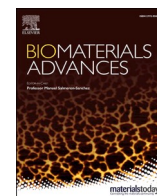# Central Lancashire Online Knowledge (CLoK)

Title	Overcoming biological barriers BBB/BBTB by designing PUFA functionalised lipid-based nanocarriers for glioblastoma targeted therapy
Type	Article
URL	https://clok.uclan.ac.uk/id/eprint/49331/
DOI	https://doi.org/10.1016/j.bioadv.2023.213660
Date	2023
Citation	Zwain, Tamara, Alder, Jane Elizabeth, Zwayen, Suha Aqeel abdulmunem, Shaw, Andrew, Burrow, Andrea Julie and Singh, Kamalinder (2023) Overcoming biological barriers BBB/BBTB by designing PUFA functionalised lipid-based nanocarriers for glioblastoma targeted therapy. Biomaterials Advances, 155.
Creators	Zwain, Tamara, Alder, Jane Elizabeth, Zwayen, Suha Aqeel abdulmunem, Shaw, Andrew, Burrow, Andrea Julie and Singh, Kamalinder

It is advisable to refer to the publisher's version if you intend to cite from the work.
https://doi.org/10.1016/j.bioadv.2023.213660

For information about Research at UCLan please go to http://www.uclan.ac.uk/research/

Overcoming biological barriers BBB/BBTB by designing PUFA functionalised lipid-based nanocarriers for glioblastoma targeted therapy

Tamara Zwain [a,b], Jane Elizabeth Alder [a], Suha Zwayen [a,c], Andrew Shaw [a], Andrea J. Burrow [a,b], Kamalinder K. Singh [a,b,*]

[a] School of Pharmacy and Biomedical Sciences, University of Central Lancashire, Preston PR1 2HE, United Kingdom
[b] Biomedical Evidence based Transdisciplinary (BEST) Health Research Institute, University of Central Lancashire, Preston PR1 2HE, United Kingdom
[c] Precision NanoSystems, 50 655 West Kent Avenue North, Vancouver, British Columbia V6P 6T7, Canada

ARTICLE INFO

ABSTRACT

A major obstacle for chemotherapeutics in Glioblastoma (GB) is to reach the tumour cells due to the presence of the blood-brain barrier (BBB) and chemoresistance of anticancer drugs. The present study reports two poly-unsaturated fatty acids, gamma-linolenic acid (GLA) and alpha-linolenic acid (ALA) appended nanostructured lipid carriers (NLCs) of a CNS negative chemotherapeutic drug docetaxel (DTX) for targeted delivery to GB. The ligand appended DTX-NLCs demonstrated particle size < 160 nm, PDI < 0.29 and a negative surface charge. The successful linkage of GLA (41 %) and ALA (30 %) ligand conjugation to DTX- NLCs was confirmed by diminished surface amino groups on the NLCs, lower surface charge and FTIR profiling. Fluorophore labelled GLA-DTX-NLCs and ALA-DTX-NLCs permeated the *in-vitro* 3D BBB model with Papp values of 1.8×10^{-3} and 1.9×10^{-3} cm/s respectively. Following permeation, both formulations showed enhanced uptake by GB immortalised cells while ALA-DTX-NLCs showed higher uptake in patient-derived GB cells as evidenced in an *in-vitro* 3D blood brain tumour barrier (BBTB) model. Both surface functionalised formulations showed higher internalisation in GB cells as compared to bare DTX-NLCs. ALA-DTX-NLCs and GLA-DTX-NLCs showed 13.9-fold and 6.8-fold higher DTX activity respectively at 24 h as indicated by IC_{50} values when tested in patient-derived GB cells. ALA-DTX-NLCs displayed better efficacy than GLA-DTX-NLCs when tested against 3D tumour spheroids and patient-derived cells. These novel formulations will contribute widely to overcoming biological barriers for treating glioblastoma.

1. Introduction

Brain tumour is a disease in which cells grow uncontrollably in the brain. Glioblastoma (GB) is a grade IV brain tumour and the most aggressive type of brain cancer, which is characterised by a heterogeneous population of cells that are highly infiltrative, angiogenic and resistant to chemotherapy [1]. The chemotherapeutic effect on GB is often limited due to the low permeability of drugs and delivery systems across the blood-brain barrier (BBB) and poor penetration into the tumour tissue [2].The BBB prevents most treatments from entering brain tissue because of its tight junctions (TJs) [3]. Docetaxel (DTX) has long been used to treat various types of cancers including breast, prostate head and neck, and gastric carcinoma with Taxotere®, the commercial dosage form approved by the FDA [4]. However, DTX a P-glycoprotein (P-gp) substrate is subject to P-gp efflux at the BBB and therefore unable to accumulate in the brain at concentrations sufficient to treat brain

metastases or primary tumours [5]. Moreover, highly functional efflux transporters and barrier properties of blood brain-tumour barrier (BBTB) further limits the drug permeation [6].

DTX like most anticancer drugs, its clinical application in GB is hindered due to its poor brain permeability, nonselective delivery, and rapid systemic clearance, which critically affect its therapeutic efficacy. Therefore, we recently reported functional nanostructured lipid carriers (NLCs) of DTX with high drug encapsulation and BBB penetrating properties [7]. NLCs are second generation of lipid nanoparticles (NPs) proposed to overcome the limitations of solid lipid nanoparticles (SLN) [8], by making the structure of solid lipid core less organised by mixing a variety of liquid lipids with solid lipids to improve drug payloads, decrease drug expulsion, improve physical and chemical stability, and offer prolonged release [9]. Functionalisation of NPs surface with different types of ligands is usually desirable to achieve selective cellular binding and internalisation through receptor-mediated endocytosis.

Some challenges of targeting cancers and tumours, as defective cells often have similar characteristics to the surrounding non-cancerous cells, to overcome this feature the ligands can be designed to have specificity and selectivity for some receptors overexpressed on cancerous cells but are less expressed on non-cancerous cells.

Polyunsaturated fatty acids (PUFAs) are bioactive lipids which have shown therapeutic potential in inflammation and cancer [10]. PUFAs have shown to induce cell apoptosis and significantly reduce the anti-oxidant content of the tumour cells [11,12]. Gamma-linolenic acid (GLA) an omega-6 eighteen carbon chain fatty acid has a potential anticancer effect in GB [11]. GLA demonstrated tumoricidal action towards GB cells with less or no neurotoxicity towards non-cancerous brain cells. It was shown that GLA's tumoricidal effect may be due to the induced apoptotic effect on GB cells [13]. Miyake et al., showed an increased number of apoptotic cells and fewer proliferative and migratory cells with GLA when studied in C6 rat glioma and T98G human glioma cells [14]. GLA produce mitochondrial depolymerisation, lipid accumulation and overexpression of P53 and GMYC, by forming various lipid peroxidase [15,16]. Limited open label clinical studies have shown that intra-tumoral injection of GLA induced significant reduction of glioma without any significant side effects [17]. Similarly, Alpha-linolenic acid (ALA) an omega-3 fatty acid has much potential for improving the therapeutic efficacy of anticancer drugs to treat various types of cancer when conjugated with chemotherapeutic drugs [18,19]. Several studies have demonstrated that ALA sensitises tumour cells to effects of anticancer drugs either in tumour-bearing animals or *in-vitro* cell culture where ALA can play an essential role in cancer prevention/progression. ALA induced changes in tumour fatty acid composition resulted in increased sensitivity to chemotherapy, especially in tumour cell lines that are resistant to chemotherapy and caused high cytotoxicity to tumour cells and protection of normal cells [20].

Fatty acid-binding proteins (FABPs) are involved in the binding, internalisation, and intracellular trafficking of fatty acids to different subcellular compartments: cytoplasmic, for metabolism and energy production, or nuclear, for the regulation of gene transcription *via* activation of peroxisome proliferator-activated receptors (PPARs) [21]. Moreover, glioma cells displayed change in the phospholipids pattern and composition in the cell membrane when treated with GLA. Interestingly, FABPs are highly upregulated in GB cells in comparison with normal brain cells thus making PUFAs a highly potential moiety for surface functionalisation of NPs for GB targeting [22,23]. Active targeting exploits the bio-functionalisation of the NPs surface by using ligands with a strong affinity and specificity for overexpressed receptors and molecules on the tumour cells [24]. Fatty acid transporters, such as fatty acid transport protein (FATP)-1, FATP-4, and fatty acid translocase/CD36 are expressed in human brain micro vessel endothelial cells which facilitate the entry of fatty acids into the brain [25]. Thus, PUFAs could be attractive and safe brain targeting ligands to enhance permeation of NPs across the BBB. Hence, surface modification of NPs with PUFAs especially GLA and ALA could represent a powerful strategy to successfully develop specific and biocompatible nano-platforms for precise and sensitive GB therapy.

In the present work DTX-NLCs were functionalised with GLA and ALA to study their potential effect on enhancing the anticancer effect of DTX improve GB targeting and to tackle essential issues related to BBB/BBTB penetration and GB uptake by assessing them through 3D *in-vitro* BBB and BBTB/GB *in vitro* disease models developed from all human primary cell lines, and immortalised GB cell line or/GB patient-derived short-term culture. Furthermore, the biofunctionalised DTX-NLCs were assessed using 3D immortalised and various 2D immortalised and patient-derived short-term culture cells for cell uptake, mechanism of cellular internalisation, cell proliferation, cell cycle arrest and cell respiration for their mitochondrial effect. To best of our knowledge this is the first report of PUFAs being investigated as surface functionalising ligands for targeting GB to improve the efficacy and internalisation of the NLCs loaded with a CNS negative drug.

2. Materials and methods

2.1. Chemicals and reagents and cell culture materials

Dynasan®114 gift sample from IOI Oleo GmbH, Germany, Phospholipon 90H, and Lipoid S75 kind gift from Lipoid, Germany. Labrasol, Lauroglycol 90 and Capryol propylene glycol monocaprylate (CPGMC) were gift samples from Gattefossé, France. Tetrahydrofuran (THF), water, acetonitrile (HPLC grade), orthophosphoric acid, dimethyl sulfoxide (DMSO), ethanol, 1-ethyl-3-(3-dimethylaminopropyl) carbodiimide (EDC), N-hydroxysuccinimide (NHS), Presto blue, 16 % formaldehyde, trypsin solution 10X, Trypan blue, trinitrobenzene sulfonic acid (TNBS), HBSS 1X, RNAs, 1X TryPLE Express, Amicon 3 kDa molecular cut-off centrifugal filters, nystatin and cytochalasin B, sodium bicarbonate (NaHCO3) solution, L-valine and hydrochloric acid solution are all purchased from Fisher Scientific, UK. Docetaxel (DTX) was purchased from Kemprotec, UK. Phosphate buffer saline (PBS) 0.1 M (pH 7.4), rhodamine 123 (R123), sodium cholate, Kolliphor®HS15 (KHS15), gamma-linolenic acid (GLA) and alpha-linolenic acid (ALA), propidium iodide, sucrose, fibronectin, trichloroacetic acid (TCAA), Evans blue dye (EBD) and agarose were purchased from Sigma Aldrich, UK. Vectashield mounting medium with DAPI was purchased from Vector Labs, UK. Accumax™ solution purchased from Merck, UK. Spectra/Por® dialysis membrane (3.5 K Da MWCO) was obtained from Spectrum Labs, USA. Seahorse kit and XF assay medium (modified DMEM, pH 7.4) purchased from Agilent, UK.

Media supplements [Foetal bovine serum (FBS), L-glutamine, sodium pyruvate, non-essential amino acid (NEAA)], Eagle's minimum essential medium (EMEM), human serum (HS), endothelial basal media (EBM-2)/(EGM-2), astrocyte basal media (ABM-2)/(AGM-2) kits were purchased from Lonza, Belgium and pericyte medium (PM), was purchased from Caltag Medsystems. SVG P12 (human, non-cancerous foetal glial cell line), U87MG (human glioblastomas, grade IV cell line) from the European Collection of Cell Cultures (ECACC, UK). BTNW911, a short-term culture derived from primary cells obtained from a 60-year-old male grade IV glioblastoma, with written ethical consent from the Brain Tumour Northwest (BTNW) tissue bank. Human microvascular endothelial cells (HMBEC), human brain vascular pericytes (HBVP), and human astrocytes (HA) were purchased from (Sciencell, Buckingham, UK). Cells were incubated in a humidified incubator under 5 % CO2 at 37 °C for culturing.

2.2. Docetaxel nanostructured lipid carrier (DTX-NLCs) production, surface modification and drug quantification

2.2.1. DTX-NLCs preparation

NLCs loaded with DTX were prepared by hot homogenisation technique [7]. Briefly, DTX (100 mg) was added to the lipid phase (Dynasan®114, Phospholipon 90H, Lipoid S75 and an equal ratios of liquid lipids) melted under controlled temperature (70 °C). The lipid phase was mixed with pre-heated (70 °C) aqueous phase composed of sodium cholate and 100 ml of distilled water under continuous stirring for 20 min to form a pre-emulsion, followed by sonication using a Probe sonicator (Vibra Cell Sonics, USA) (intensity of 40 %) under controlled temperature, and then allowed to congeal at room temperature to form DTX-NLCs.

The Blank NLCs (B-NLCs) was prepared following the same protocol without adding the DTX to the lipid phase. For Rhodamine 123 tagged NLCs, the fluorescence dye was added into the melting lipid phase, and a similar method was carried out for the size reduction process to form R-DTX-NLCs.

2.2.2. NLCs surface modification with GLA/ALA

The DTX-NLCs were surface modified with either GLA or ALA using 1-ethyl-3-(3-dimethylaminopropyl) carbodiimide (EDC) and N-hydroxy succinimide (NHS) as coupling agents (Fig. 1a) [26]. Briefly, GLA/ALA
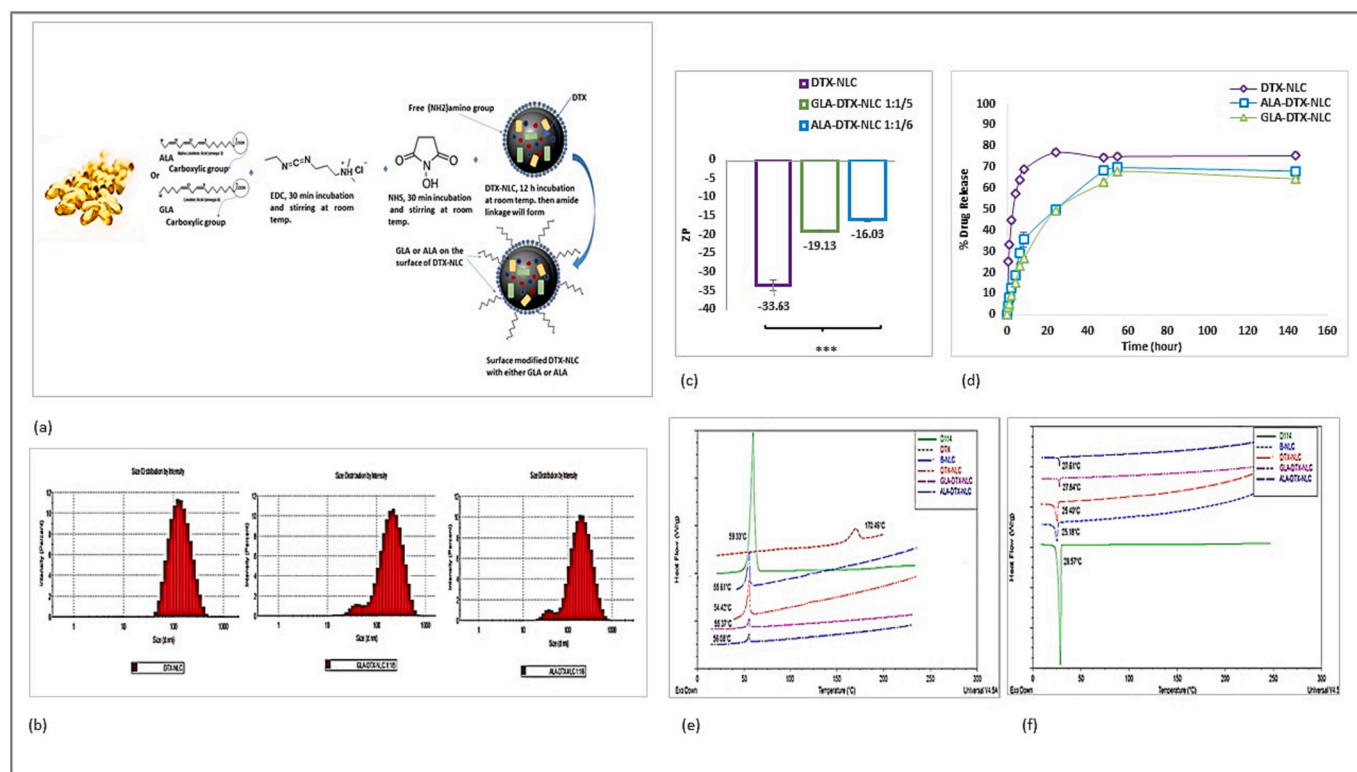
Fig. 1. (a) Schematic diagram showing the crosslinking of DTX-NLCs with PUFAs by covalent bonding in the presence of EDC and NHS to form an amide linkage between a free amino group of DTX-NLCs and PUFAs carboxylic group. This reaction was carried out at room temperature (Chemical structures were adopted from Fisher and Sigma, UK websites), (b) Particle size distribution of DTX-NLCs, GLA-DTX-NLCs and ALA-DTX-NLCs, (c) Zeta potential for DTX-NLCs as compared to GLA-DTX-NLC 1:1/5 and ALA-DTX-NLC 1:1/6 FAG: PUFA ratios, (d) DTX release profile from NLCs over the period of 144 h at 37 °C, (e) and (f) DSC thermographs using method heat/cool/heat, for Dynasan 114, DTX, DTX-NLCs, B-NLCs, GLA-DTX-NLCs and ALA-DTX-NLCs. Data are mean ± SD, $N = 3$. Data are mean ± SD, N=3, *** P < 0.000 refers to the significant difference when compared to Zeta potential of GLA-DTX-NLCs and ALA-DTX-NLC formulations.

were dissolved in ethanol, then mixed for 30 min with EDC dissolved in water pH 7.4. The PUFA: EDC were mixed in 1:1 M ratio and mixing was carried under nitrogen gas to maintain the stability of PUFAs. This was followed by addition of NHS also at molar ratio of 1:1 under continuous stirring for further 30 min. Finally, 1 ml DTX-NLC formulation was added to the mixture under a stream of nitrogen gas and kept under stirring for up to 12 h to form GLA-DTX-NLC or ALA-DTX-NLC, respectively (Fig. 1a). Free amino groups (FAG) on the DTX-NLCs were determined (Section 2.2.3) and various ratios of FAG to PUFA were investigated to obtain the optimized surface functionalisation. For preparation of rhodamine 123 tagged formulations (R-GLA-DTX-NLC and R-ALA-DTX-NLC), R-DTX-NLCs was used for surface functionalisation with respective PUFAs. Excessive unbound GLA/ALA was removed using dialysis for three purification cycles. Photon correlation spectroscopy (PCS) was used to obtain the particle size, polydispersity index (PDI), and zeta potential (ZP) of bare and surface modified DTX-NLCs using Zeta Sizer Instrument at 25 °C (Malvern Zetasizer Nano, Malvern Panalytical Ltd., UK).

2.2.3. Determination of free amino group (FAG) and Conjugation efficiency

Conjugation efficiency was calculated by determining FAG on DTX-NLCs pre- and post-conjugation with ligands (GLA/ALA). Since FAG

react with trinitrobenzene sulfonic acid (TNBS), therefore, TNBS was used to determine FAG on DTX-NLCs surface. The TNBS was added to the formulation, and the reacted TNBS measures the FAG in the tested samples as per the modified method reported by Gao et al. [27]. The reacted TNBS was calculated by Eq. (1).

$$Reacted\ TNBS = Total\ TNBS - Unreacted\ TNBS \qquad (1)$$

Briefly, 0.5 ml of each NLC formulation was added to an appropriate volume of TNBS (4 μmol/ml) and incubated for 1 h at 40 °C in a dark place. Samples were then centrifuged for 30 min at 16,300 ×g and supernatant was placed in two individual volumetric flasks, one was treated as the active sample (treated with 100 μl of 1 % trichloroacetic acid (TCAA)) and 100 μl of L-valine (40 μmol/ml), and the second was treated as a blank sample (treated with 100 μl of 1 % trichloroacetic acid (TCAA) only). Both samples were incubated in the dark for 1 h at 40 °C for the reaction to take place, then removed from the incubator, and the reaction was terminated by adding HCl solution. The absorbance was then measured using a UV spectrophotometer at 410 nm wavelength. The TNBS calibration curve preparation for a range of concentrations is detailed in the supplementary data. The % ligand conjugation to DTX-NLCs was calculated using Eq. (2).

$$\%Conjugation = \left\{ \frac{Total\ FAG\ before\ conjugation - FAG\ after\ conjugation}{Total\ FAG\ before\ conjugation} \right\} *100 \qquad (2)$$

2.2.4. Quantification of drug loading and entrapment efficiency

The quantification of DTX in pre- and post functionalised DTX-NLCs was determined by using a validated HPLC method, with pre-optimized chromatography condition. Chromatography was carried out using Phenomenex column Luna 5 μm, PFP [2], 100 Å, 250 × 4.6 mm (Phenomenex, UK) on Agilent HPLC 1260 Infinity system (Agilent Technologies, USA,) with UV detector set at wavelength 230 nm. HPLC runs were performed using acetonitrile and water isocratic mobile phase (50:50, v/v), at a flow rate of 1.0 ml/min, sample injection volume of 20 μl and the column temperature adjusted to 40 °C for the total analytical period of 15 min. The NLCs were dissolved using a serial dilution of THF and mobile phase (acetonitrile and water, 50:50, v/v), then placed in HPLC vials for an analytical run to calculate the percent drug loading (% DL) and total drug (%TD) using Eq. (3) and (4), respectively. The entrapment efficiency (EE) was determined by quantifying free DTX (FD) concentration in the filtrate separated from NLCs by placing the formulation in an Amicon 3 kDa molecular cut-off centrifuge filters and centrifuged at 15,600 ×g for 60 min. The percent entrapment efficiency (%EE) was determined by Eq. (5) [7]

$$\%DL = \left\{ \frac{mass \ of \ DTX}{mass \ of \ Lipids \ in \ the \ NLCs + mass \ of \ DTX} \right\} \times 100 \qquad (3)$$

$$\%TD = \left\{ \frac{DTX \ concentration \ after \ processing}{DTX \ added \ concentration \ before \ processing} \right\} \times 100 \qquad (4)$$

$$\%EE = \left\{ \frac{TD - FD}{TD} \right\} \times 100 \qquad (5)$$

2.3. Docetaxel NLCs physicochemical characterisation

2.3.1. In-vitro DTX-NLCs release

The DTX release pattern from pre- and post functionalised DTX-NLCs were evaluated in phosphate buffer saline (PBS) pH 7.4 containing 30 % (v/v) ethanol as release media. Samples were placed in the dialysis membrane molecular weight cut-off 3.5 kDa bags and immersed in 400 ml of release media at 37 °C under shaking at 100 rpm/min. An appropriate volume was withdrawn at a predetermined time points and replaced with the exact volume of fresh release media to maintain the sink conditions. DTX was quantified in the samples by a validated HPLC method and the drug release experiment was performed for a period of 144 h.

2.3.2. Thermal behaviour study by Differential scanning calorimetry (DSC)

DSC was used to evaluate the crystallisation and melting behaviour of lipid and DTX in pre- and post functionalised formulations on Q2000 DSC (TA Instruments, Cheshire, UK). Sample was placed in a hermetically sealed Tzero pan, and an empty pan was used as a reference and analysed using heat/cool/heat (10 °C/min and the temperature was cycled between 0 and 240 °C). Samples were measured under a nitrogen purge of 50 ml/min. The data collected and analysed using TA Universal Analysis software (TA Instruments, UK).

2.3.3. Fourier-Transform Infrared (FTIR) spectroscopy

FTIR were used to determine material interactions and changes between pre- and post functionalised DTX-NLCs. FTIR (Nicolet iS 10 Fourier transform infrared spectroscopy, Thermo scientific, UK) was employed using % transmittance ranging between 400 and 4000 cm^{-1} by a diamond crystal and a resolution of 0.5 cm^{-1} and accumulation of 150 scan.

2.4. In-vitro cell line studies

2.4.1. Permeability and GB uptake evaluation through 3D in-vitro BBB and BBTB models

The pre and post functionalised DTX-NLCs were evaluated for their permeability through BBB and BBTB *in-vitro* models developed from all human origin primary cell lines. The BBB was established by modifying the published protocol [28,29]. Briefly, the HA and HBVP cells were seeded on the basal part of the insert followed by seeding HBMEC on the apical part of the insert, and the media was replenished accordingly. The plates were then incubated for 48 h at 37 °C. Once the BBB model was established, and the trans-endothelial electrical resistance (TEER) values were in the range of ~250 Ω/cm^2, the tumour GBs were introduced to form the BBTB, either immortalised U87MG cells or patient-derived short-term culture BTNW911 were seeded on the base of the plate [7].The Rhodamine 123 tagged DTX-NLCs (R-DTX-NLCs, R-GLA-DTX-NLCs and R-ALA-DTX-NLCs) were diluted with equal mix ratio of media and incubated on the apical side of the models for predetermined time points. At the end of each time point, an appropriate volume was withdrawn from the basolateral side for analysis. The fluorescence was measured at λ_{Ex} 485 nm, and λ_{Em} 535 nm using plate reader (Genios Pro microtiter plate reader, Tecan, Austria). The TEER was measured using EVOM-2 instrument (World Precision Instruments Ltd, Hertfordshire, UK) and flow cytometer were used to quantify GB cell uptake following permeation through the BBB model. The U87MG/BTNW911 cells in BBTB model were collected from the base of the transwell, and samples were prepared and analysed by flow cytometer (Gauva, Merck, Germany). Evans blue dye (EVD) was used prior and at the end of each experiment to establish the integrity of the model. The apparent permeability (Papp) of all formulations was obtained by Eq. (6).

$$P_{app} = \left(\frac{V}{A \times C_0} \right) \times \left(\frac{dQ}{dt} \right) \qquad (6)$$

where:V = Volume of basolateral compartment (0.5 cm^3), A = Surface area of the polycarbonate membrane (0.3 cm^2), C$_0$ = Concentration of formulations in the apical side, dQ = Change in the concentration of formulation passing across the cell layer to basolateral side (μg/ml), dt = Change in time (s).

2.4.2. Qualitative and quantitative cellular internalisation

The cellular internalisation mechanism for entry of R-DTX-NLCs, R-GLA-DTX-NLCs and R-ALA-DTX-NLCs was evaluated in U87MG and SVG P12 cells. For qualitative uptake, images were captured with the Zeiss fluorescence microscope in a 63× magnification with an oil lens and processed with Zen blue software (Carl Zeiss Microscopy GmbH, Germany). The cells were seeded on sterile coverslips and placed in a 12-well plate then incubated for 24 h. The plates containing the adherent monolayer cells (seeded on the coverslips) were then washed twice with pre-warmed PBS (0.1 M, pH 7.4) and treated with NLCs diluted with fresh media and incubated for 2 h, then washed three times with PBS. Cells were then fixed by 4 % paraformaldehyde diluted with PBS (1:4 ratio, v/v), followed by adding mounting medium containing DAPI to stain the nucleus on the microscope slide, the coverslips containing the cells were placed facing down on the slide then sealed with nail polish and stored overnight at 4 °C in a slide box.

The quantitative uptake studies were performed using flow cytometer (Guava, Merck, Germany) and the analysis carried out with Guava® EasyCyte software 3.1.1 (Guava, Merck, Germany). The 3D U87MG spheroids were prepared as per previous report by Zwain et al. [7], and the monolayer U87MG, SVG P12 and BTNW911 were seeded in a 12-well tissue culture plate and cultured for 24 h then the media were replaced with R123 tagged formulations diluted with media. The cells were evaluated for a time and concentration-dependent uptake studies, following each designated time point, PBS (0.1 M, pH 7.4) was used to wash the cells. The monolayer cells were trypsinised/3D spheroids were dissociated by AccuMax® cell then centrifuged at 179 ×g for 5 min. The cell pellet was resuspended with ice-cold PBS and placed in non-tissue culture V-shaped 96 well plates then treated with propidium iodide (PI) (50 μg/ml stock) prior to the analysis.

2.4.3. Quantitative and qualitative endocytosis pathways evaluation

Following the same protocol mentioned for the quantitative and qualitative uptake study using flow cytometer and fluorescence microscopy in Section 2.4.2, the U87MG and SVG P12 cells were seeded and incubated to different endocytosis inhibitors diluted with media. The inhibitors were: incubation at 4 °C used for energy-dependent endocytosis, 5 µg/ml cytochalasin B used for micropinocytosis/phagocytosis, 5 µg/ml nystatin used caveolae/lipid rafts pathway and 0.45 M sucrose used for clathrin pathway for 90 min. Media containing endocytic inhibitors was removed and replaced with R123-labelled formulations (R-DTX-NLC, R-GLA-DTX-NLC and R-ALA-DTX-NLC) diluted with media plus the inhibitors mentioned above and further incubated for 4 h. Samples were then prepared and analysed to determine which pathway each formulation was utilizing to gain entry to the cells.

2.4.4. Cell proliferation in 2D cell lines and 3D spheroids

The U87MG, SVG P12 and BTNW911 cell lines in 2D models and U87MG 3D spheroids were seeded in a 96-well plate. Media without cells was used as a blank, and cells and media without a drug were used as a control. The monolayer cell lines were then cultured for 24 h prior to treatment with the drug solution, and surface-modified DTX-NLCs with ALA/GLA were diluted with media and incubated to establish a dose and time-dependent toxicity effect. The cells were treated with Presto Blue® to perform the proliferation assay and incubated for 1 h, then fluorescence response for Presto Blue at λ_{Ex} 535 nm and λ_{Em} 612 nm was detected, and cell proliferation that is corresponding to cell viability was calculated using Eq. (7).

(modified DMEM, pH 7.4, Agilent), containing glucose (25 mmol/L), glutamine 2 (mmol/L), and sodium pyruvate (2 mmol/L), before being incubated for another hour. Oxygen consumption rate (OCR) was determined using the XFp analyser (Seahorse Bioscience). Basal OCR measurements were measured followed by injection of the following compounds (prepared fresh from the XF Cell Mito Stress Test Kit (Agilent): oligomycin (1 µmol/L, injection port A)), FCCP (1 µmol/L, injection port B), and combined antimycin A (0.5 µmol/L), and rotenone (0.5 µmol/L) (injection port C). Data obtained were normalised to protein concentration, determined *via* BCA assay.

2.5. Statistical analysis

The Kolmornov-Smirnov test for normality was used followed by ANOVA (with post-hoc analysis Tukey and Dunnett test) SPSS Version 20 software (IBM Company, USA) and the Microsoft Excel software for Microsoft office 360 (Microsoft Corporation, USA). The analysis of variance was considered as statistically significant (*) when the difference $P < 0.05$ (level of confidence 95 %), (**) $P < 0.01$ (level of confidence 99 %), and (***) $P < 0.001$ (level of confidence 99.99 %). The collected data presented as the mean $\pm$ standard deviation (SD) for $N=3$.

3. Results

3.1. NLCs production, surface modification and drug quantification

Following cross-linking with the PUFAs through EDC-NHS coupling

$$\%\textbf{\textit{Cell}}\ \textbf{\textit{Viability}} = \left[\frac{(\textbf{\textit{Fluorescence of DrugTreatment}} - \textbf{\textit{Fluorescence of Blank}})}{(\textbf{\textit{Fluorescence of Control}} - \textbf{\textit{Fluorescence of Blank}})} \right] \times \textbf{100} \tag{7}$$

Mean cell viability *versus* drug concentration was plotted using the Prism5 software (GraphPad Software, USA). IC$_{50}$ values were calculated as the concentration at which 50 % inhibition (decrease in cell proliferation) was achieved.

2.4.5. Cell cycle analysis

Cell cycle analyses were performed by PI staining to evaluate the effect of DTX solution, DTX-NLCs, GLA-DTX-NLCs and ALA-DTX-NLCs on the cell cycle distribution. The U87MG cells were seeded in 12-well tissue culture plates and kept in the incubator overnight for culturing. Then, the media was replaced by above mentioned treatments followed by incubation for 24 h. Following treatment, the cells were washed, trypsinised, and centrifuged at 179 $\times g$ for 5 min. The cell pellets were resuspended and fixed by adding ice-cold 70 % ethanol (diluted with PBS). The fixed samples were centrifuged at 179 $\times g$ for 5 min and washed with ice-cold PBS, then centrifuged again at 179 $\times g$ for 5 min. The fixed cells were resuspended with PBS and transferred to non-tissue culture plates. PI concentration (500 µg/ml stock) was added to each well, followed by adding RNAase (10 mg/ml) and incubated for 2 h followed by testing the samples by flow cytometer. The Guava software was used for data analysis to determine DNA content by fluorescence intensity (488 nm).

2.4.6. Seahorse experiment

XFp culture plates were used to seed the cells, and the plates were incubated overnight to allow the cells to attach and proliferate. The cells were treated with bare, and surface modified formulations diluted with fresh medium and incubated for further 24 h, the cells with no treatment were considered as a control. Following the treatment, cells were washed, and culture medium was replaced with XF assay medium

(Fig. 1a), particle size of DTX-NLCs (123.30 $\pm$ 0.64 nm, Supplementary data Fig. S1a) increased depending upon the ligand density. FAG on the surface of the DTX-NLCs were quantified to optimize their coupling to GLA and ALA. For GLA-DTX-NLCs when FAG: GLA, ratio was increased 1:1/5, 1:1/4, 1:1/3, 1:1/2, and 1:1 for coupling, particle size was found to increase almost linearly (160–452 nm) (Supplementary data Fig. S1a). Finally, GLA-DTX-NLCs with FAG:GLA ratio of 1:1/5, mean particle size of 157.36 $\pm$ 1.53 nm and ALA-DTX-NLCs with FAG: ALA ratio of 1:1/6, mean particle size 155 $\pm$ 0.10 nm were selected because of their lower particle size (Table 1) and higher antiproliferative activity (Table S3). Both formulations with particle size increase of ~30 nm as compared to bare DTX-NLCs revealed homogenous dispersity as characterised by PDI values of < 0.29 (Fig. 1b). DTX-NLCs displayed zeta potential of -32.4 ± 0.96 mV which was significantly reduced to -19.13 ± 0.20 and -16.03 ± 1.20 mV for GLA-DTX-NLCs and ALA-DTX-NLCs respectively confirming surface functionalisation (Table 1) (Fig. 1c). Furthermore, DTX-NLCs (FAG 6.23 $\pm$ 0.69 µmol/ml) were reduced after coupling with GLA (FAG 3.38 $\pm$ 0.51 µmol/ml) and ALA (FAG 4.025 $\pm$ 0.27 µmol/ml) confirming 41 % and 30 % conjugation respectively for GLA-DTX-NLCs and ALA-DTX-NLCs respectively (Table 1). DTX-NLCs showed a high entrapment efficiency (>98 %) with an active drug loading (total drug content of 88 %), while the functionalisation had no effect on entrapment efficiency of the drug. The total drug showed a slight reduction for both GLA-DTX-NLCs (66.98 %) and ALA-DTX-NLCs (62.41 %) (Table 1), due to dilution during functionalisation process.

Table 1

Physicochemical characterisation data for DTX-NLCs and DTX-NLCs surface-modified formulations. Data mean values ±SD (N=3).

Formulation Batches	Mean particle size (nm)	Poly dispersity index	Zeta potential (mV)	Free amino acid group (FAG) concentration (μmol/ml)	Ligand conjugation (%)	Entrapment efficiency (%)	Total drug (%)	Drug loading (%)
DTX-NLCs	123.30 ±0.64	0.230 ±0.642	−32.40 ±0.96	6.23 ±0.69	–	99.13 ±1.20	88.60 ±1.37	2.01 ±0.03
GLA-DTX-NLCs	157.36 ±1.53	0.271 ±0.004	−19.13 ±0.20	3.38 ±0.51	41 ±2.39	98.67 ±0.20	66.98 ±7.73	1.35 ±0.17
ALA-DTX-NLCs	155 ±0.10	0.289 ±0.007	−16.03 ±1.20	4.02 ±0.27	30 ±3.14	99.21 ±0.42	62.41 ±4.70	1.25 ±0.08

3.2. NLCs physicochemical characterisation

#### 3.2.1. In-vitro drug release

The cumulative drug release of DTX from the functionalised DTX-NLCs exhibited controlled drug release at pH 7.4, indicating that the presence of GLA/ALA on the outer layer of the DTX-NLCs surface influenced the DTX release. The release pattern of GLA-DTX-NLCs and ALA-DTX-NLCs showed an initial slow with ~12 % of DTX released from each of the formulation at 2 h, followed by sustained release with 40 % drug released at 24 h and ~62 % and 68 % of DTX released from GLA-DTX—NLCs and ALA-DTX-NLCs respectively at 48 h after which the drug release plateaued with ~64 and 68 % of DTX released from GLA-DTX-NLCs and ALA-DTX-NLCs respectively at 144 h (Fig. 1d). This constrained release from surface modified nanoparticles has been previously reported where increased distance between the surface and core of the NLCs consisting of drug and lipid blend could be the contributing factor [30–32]. In comparison the free surface of DTX-NLCs lead to a faster drug release than GLA/ALA functionalised formulations. More than 40 % of the DTX was released from DTX-NLCs at 2 h presenting a biphasic release profile with the initial fast burst release followed by a slow, sustained release.

3.2.2. Thermal behaviour studies by Differential scanning calorimetry (DSC)

DSC thermographs revealed in the pre and post functionalised formulations that DTX might be present in an amorphous state or in a solid-solution state after encapsulation into the NLCs (Fig. 1e and f), since no characteristic DTX peak was observed in all NLCs at 170 °C the typical melting point for DTX. The formulations exhibited an endothermic peak at ~55.37 °C, a characteristic peak of Dynasan® (D114), solid lipid used in the formulation of NLCs. Similar finding has been obtained in previous reports [33,34] and recrystallisation of lipid during the cooling cycle as shown by the exothermic ~25.18 °C.

3.2.3. Fourier-transform infrared and spectroscopy

FTIR spectra revealed that GLA-DTX-NLCs and ALA-DTX-NLCs retained all the characteristic peaks of DTX-NLCs. In addition, they showed characteristic peaks of GLA and ALA at (1772, 1775, 1506, 1419, and 917) cm^{-1} that were related to (C=O, C=O, N—H bending, CH$_2$ symmetrical, and C=C), respectively, and new peaks formed at (2991, 1085, 1044 and 882) cm^{-1} that were characterisation for (N—H stretching, C—O stretching, Aromatic deformation, C-O-C and C—H bending) respectively confirming the functionalisation (Supplementary
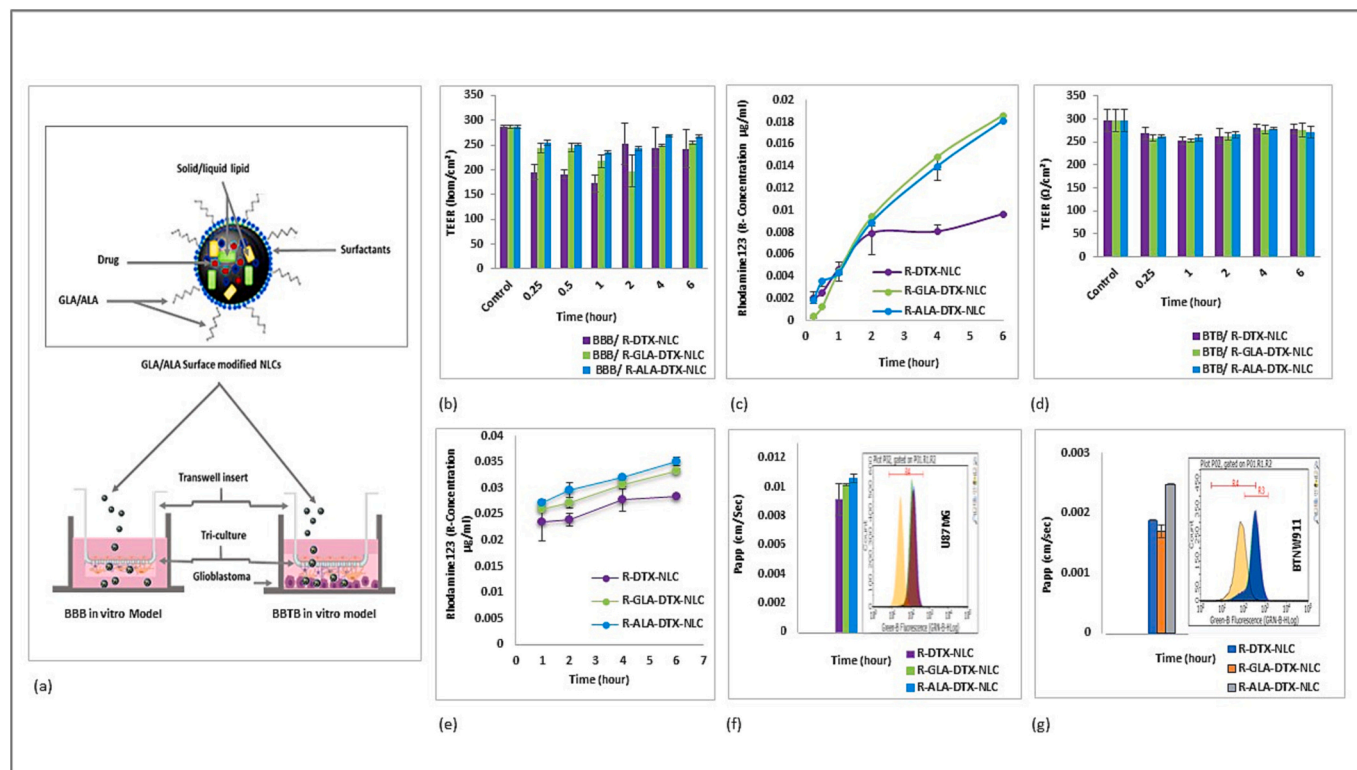
Fig. 2. (a) Illustration of PUFAs-DTX-NLC permeability and uptake across *in-vitro* BBB and BBTB models (b) and (d) graphs for the TEER measurements and (c) and (e) Fluorescence concentration in the basolateral side of transwell after treatment with R-DTX-NLCs, R-GLA-DTX-NLCs and R-ALA-DTX-NLCs across BBB and BBTB models (f) and (g) Papp and flow cytometer histograms demonstrating the U87MG/BTNW911 uptake, and peak shifts for 6 h incubation time of control (untreated U87MG cells) and 1 μg/ml of R-DTX-NLCs, R-GLA-DTX-NLCs, and R-ALA-DTX-NLCs, respectively. Data are mean ± SD, (*N*=3).

data Fig. S1b and c, Tables S1 and S2).

3.3. In-vitro cell lines studies

#### 3.3.1. Permeability and uptake evaluation through 3D in-vitro models

As illustrated in Fig. 2a, the permeation of pre- and post-functionalised NLCs through the 3D *in-vitro* models was determined, to study the brain delivery for NLCs [35]. The model was considered intact due to no EBD detectable in the basolateral side of the insert during and at the end of the experiments.

3.3.1.1. NLCs permeation through the 3D in-vitro BBB model.
R-DTX-NLCs showed paracellular permeation through an *in-vitro* BBB model as illustrated in Fig. 2a, due to the transient opening of the tight junctions (TJs), as evident by the reduction in the TEER values from control values $\sim$286.5 to 190 Ω/cm^2 at early time points (0.25–1) hour, followed by building back of the TEER values from 2 till 6 h of incubation. In addition to paracellular permeation, there may be another mechanism involved to allow the permeation of R-GLA-DTX-NLCs and R-ALA-DTX-NLCs as no evidence of a steep drop in the TEER values were observed in comparison to bare DTX-NLCs. The GLA-DTX-NLCs showed a reduction of TEER to 197 Ω/cm^2 around 2 h while the ALA-DTX-NLC TEER values were around 235 Ω/cm^2 following 1 h of incubation (Fig. 2b). However, all three formulations showed continuous permeation even after TEER values returned to typical values, with highest concentrations were displayed for both R-GLA-DTX-NLCs and R-ALA-DTX-NLCs at the 6 h as revealed by $\sim$two folds higher fluorescence measured on the basal side of the transwells as compared to bare R-DTX-NLCs with no surface modification (Fig. 2c). Following 1 h incubation time, all three formulations displayed a high permeation through the BBB *in-vitro* model as evident from high Papp 2×10^{-3}, 1.8×10^{-3}, 1.9×10^{-3} cm/s for R-DTX-NLCs, R-GLA-DTX-NLCs, R-ALA-DTX-NLCs respectively. Generally, Papp $> 60 \times 10^{-6}$ cm/min is considered high, according to Amidon

et al., and Esposito et al. [28,36].

3.3.1.2. NLCs permeation/GB uptake through 3D in-vitro BBTB models.
To further understand the fate of the formulations following permeation through the triculture BBB layer in the model, and to examine their uptake by GB cells, studies were carried out on *in-vitro* BBTB model with immortalised U87MG or the patient-derived short-term culture BTNW911 grown in the base of the 3D *in-vitro* BBB model (Fig. 2a). The BBTB model demonstrated a TEER $\sim$297.66 $\pm$ 24.20 Ω/cm^2 for the control (untreated cells), which showed a drop in the TEER values to $\sim$253.66 $\pm$ 7.96 Ω/cm^2 at 1 h, when the formulations were incubated. The TEER gradually returned close to the control values, which in turn, suggest that they interact with the TJ proteins in the endothelial barrier causing them to open transiently and might suggest the permeation of formulations through the paracellular diffusion in the presence of the GB cells (Fig. 2d). Furthermore, clearly, another mechanism might be involved with the transport of PUFA modified NLCs since the fluorescence concentration indicated a continuous passage through the model with higher permeation of R-ALA-DTX-NLCs and R-GLA-DTX-NLCs in comparison to free surface R-DTX-NLCs, starting from early time point (0.25 h) and reaching maximum permeation towards 6 h of incubation under similar conditions (Fig. 2e). This was also reflected by the Papp values demonstrating higher permeation of the R-ALA-DTX-NLCs in comparison to the other two formulations across the BBTB model in the presence of immortalised U87MG and the patient-derived short-term culture BTNW911 (Fig. 2f and g). R-GLA-DTX-NLCs exhibited lower Papp value in the presence of BTNW911 as compared to U87MG (Fig. 2f and g). The flow cytometer data further confirmed the formulations were up taken by immortalised and patient-derived short term culture GB cells following crossing the BBTB model as evident by the histograms showing peak shift in comparison to untreated control (Fig. 2f and g).
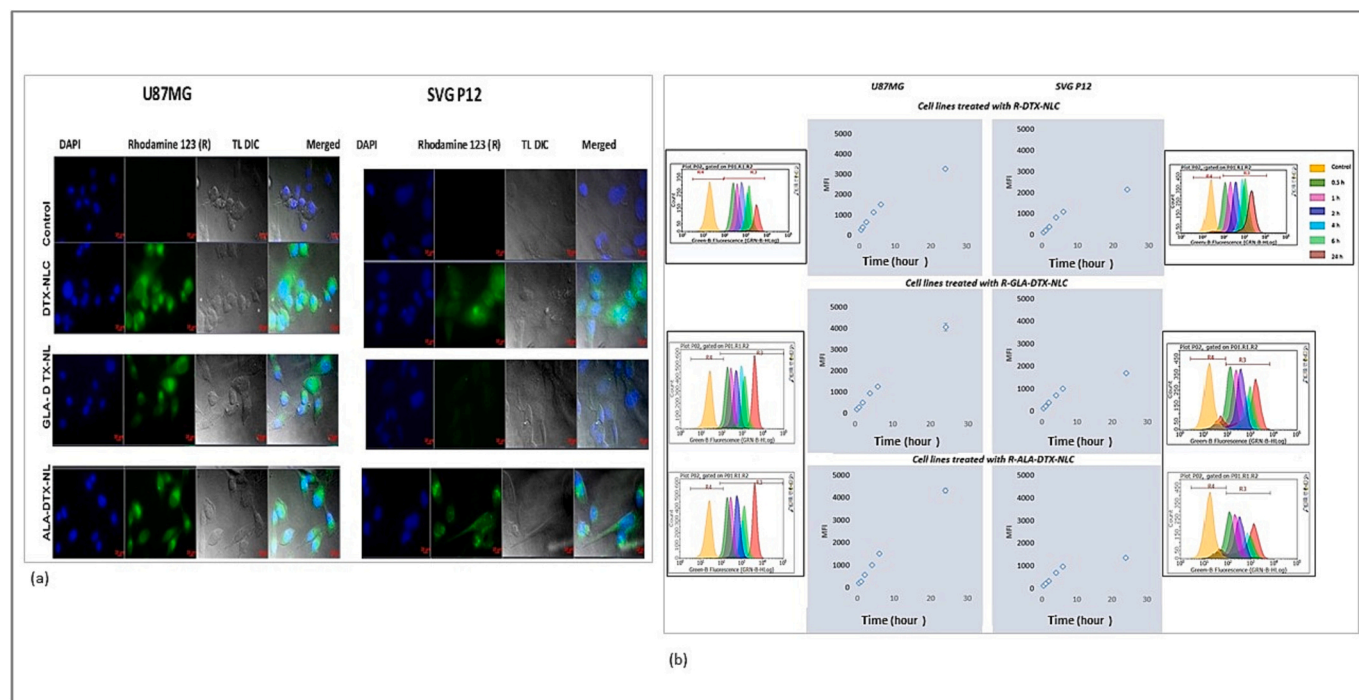
Fig. 3. (a) Cellular internalisation for U87MG and SVG P12, in the images blue colour refers to the stained nucleus with a fluorescence dye (DAPI), and the green fluorescence dye refers to NLCs formulations (Rhodamine 123) following 2 h incubation with R-DTX-NLCs, R-GLA-DTX-NLCs and R-ALA-DTX-NLCs, (b) Standard plots of best fit demonstrating the time-dependent uptake in cell lines treated with fluorescently labelled NLCs and surface modified NLCs, and flow cytometer histograms for the time-dependent uptake when cell lines were incubated for 0.5, 1, 2, 4, 6, and 24 h respectively, the R4 representing a region around the untreated control cells, and R3 representing a region around the shifted peaks as the fluorescence intensity increases the peaks shift more to the right over time as evidence of increased uptake with time. Data are mean and $\pm$SD, (N=3).
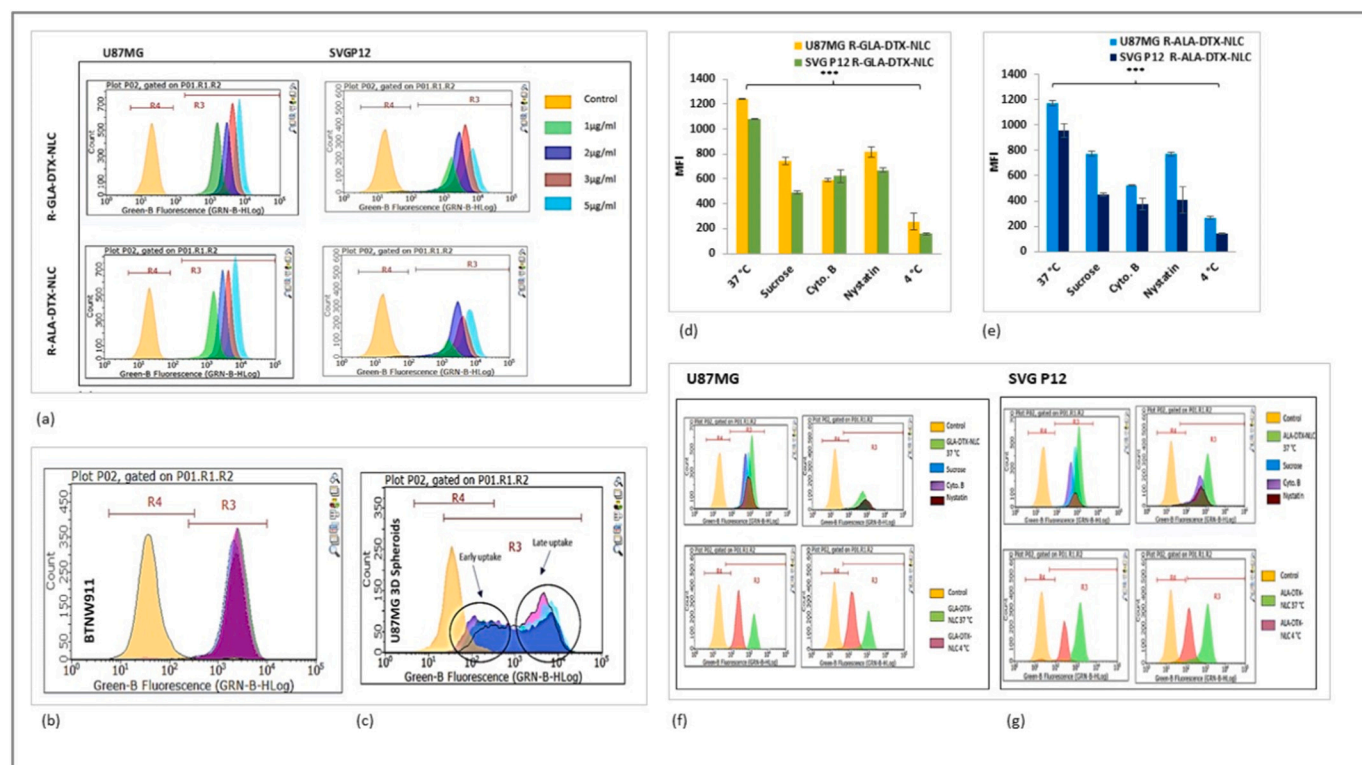
Fig. 4. (a) Flow cytometer histograms for the concentration-dependent uptake of NLCs following treatment in U87MG and SVG P12, (b) Flow cytometer histograms of BTNW911 uptake with R-DTX-NLCs, R-ALA-DTX-NLCs, and R-GLA-DTX-NLCs ▨▨▨ respectively, (c) Flow cytometer histograms for uptake through U87MG spheroids of R-DTX-NLCs, R-ALA-DTX-NLCs, R-GLA-DTX-NLCs respectively ▨▨▨ at 6 h incubation time. The ▨ control, in this case, was the untreated cell lines. (d) and (e) MFI flow cytometer for U87MG and SVG P12 cell lines treated with endocytosis pathway inhibitors pre and during incubation with R-GLA-DTX-NLCs and R-ALA-DTX-NLC,s (f) and (g) flow cytometer histograms for endocytosis pathways inhibitors before and during incubation with treatment for U87MG and SVG P12. * $p < 0.05$ and *** $p < 0.000$, refers to a very significant difference. Data are mean and $\pm$ SD, (N=3).

3.3.2. Qualitative and qualitative cellular internalisation

The qualitative internalisation images demonstrated a strong and intense green, fluorescent signal around the nucleus, and the cytoplasm when pre and post functionalised formulations were examined after incubation with U87MG cells in comparison to lower intensity observed when incubated with non-cancerous brain cells SVG P12 (Fig. 3a). Interestingly, R-GLA-DTX-NLCs showed significantly lower uptake in SVG P12 in comparison to the R-DTX-NLCs. This is in line with a previous report, demonstrating less uptake of GLA with the non-cancerous cells [37]. Furthermore, the quantitative data displayed higher time-dependent uptake over the period of 24 h with R-GLA-DTX-NLCs and R-ALA-DTX-NLCs as compared to R-DTX-NLCs with more favourable uptake in U87MG rather than SVG P12 cells (Fig. 3b). The data also indicated a concentration-dependent pattern, since the cell uptake increased as a result of increasing the concentration, PUFA functionalised NLCs showed higher uptake towards U87MG as evident from flow cytometer histograms (Fig. 4a). Additionally, all the three formulations indicated uptake with BTNW911 and 3D tumour spheroids with no significant difference amongst the formulations (Fig. 4b and c).

3.3.3. Quantitative and qualitative endocytosis pathways analysis

The internalisation mechanism in U87MG and SVG P12 cells for both R-GLA-DTX-NLCs and R-ALA-DTX-NLCs was thought to be an active energy-dependent transport as evidenced by low uptake of formulations when incubated at 4 °C as compared to the incubation of same formulations at 37 °C. These results were in line with previous reports [38]. Both the formulations demonstrated that multiple pathways were involved in the endocytosis with micropinocytosis and clathrin-mediated being the main pathways for the internalisation of GLA-DTX-NLCs in U87MG and SVG P12 (Fig. 4d and e). A similar pattern

Table 2

Mean IC_{50} values for GLA-DTX-NLCs and ALA-DTX-NLCs as compared to DTX and DTX-NLCs following 24, 48, and 72 h incubation through 2D and 3D cell line models.

Cell line	Time (hours)	IC$_{50}$ Values (ng/ml)			
		DTX	DTX-NLCs	ALA-DTX-NLCs	GLA-DTX-NLCs
U87MG	24	7.22 ±0.84	32.44*** ±2.72	11.59 ±1.39	5.46 ±0.93
U87MG	48	5.44 ±3.94	24.37*** ±0.74	2.85 ±0.32	4.50 ±0.57
U87MG	72	1.80 ±0.01	3.17 ±0.36	2.58 ±0.19	3.06 ±0.52
SVG P12	24	2.07 ±0.46	23.04*** ±6.42	10.56* ±1.79	11.82* ±1.58
SVG P12	48	2.55 ±0.58	7.10*** ±0.82	3.17 ±0.36	5.13* ±0.43
SVG P12	72	0.22 ±0.10	1.80 ±1.18	1.12 ±0.12	1.85 ±0.77
BTNW911	24	95.16 ±4.95	N/A[a]	6.82*** ±0.45	13.89*** ±1.21
BTNW911	48	10.05 ±0.32	62.71*** ±2.15	6.27* ±0.28	12.51 ±0.45
BTNW911	72	1.77 ±0.64	25.18*** ±0.24	5.97*** ±0.48	10.55*** ±0.76
3D U87MG spheroids	72	12.74 ±0.83	3.60*** ±0.53	10.02 ±0.39	37.42*** ±2.17

[a] IC_{50} value could not be obtained as the 50% of cell death was not achieved at the range of drug concentrations studied.

was observed with R-ALA-DTX-NLCs when examined in U87MG, and all three pathways were equally involved for R-ALA-DTX-NLCs uptake in the SVG P12 (Fig. 4d and e). This is also evident by the flow cytometer histogram peak shift as seen in Fig. 4f and g. A qualitative fluorescence microscopy images were also acquired to support the data, as demonstrated in Fig. S2a–d (Supplementary data).

3.3.4. Cell proliferation in 2D cell lines and 3D spheroids

The evaluation for cell toxicity is one of the crucial steps to understand the dose and time-dependent behaviour in an *in-vitro* situation. The surface appended NLCs showed lower IC_{50} values with GLA-DTX-NLCs (5.49 fold less at 48 h) and ALA-DTX-NLCs (8.55 fold less at 48 h) as compared to bare DTX-NLCs thus demonstrating improved efficacy on functionalisation which could be attributed to higher cell uptake of the functionalised NLCs. Interestingly, surface functionalised formulations were found to be safer than native drug DTX as revealed by higher IC_{50} values towards non-cancerous SVG P12 brain cells (Table 2). For BTNW911 patient-derived short-term culture, ALA-DTX-NLCs displayed higher activity (lower IC_{50}) than DTX, DTX-NLCs and GLA-DTX-NLCs at 24 and 48 h hours while GLA-DTX-NLCs exhibited more potency with significantly lower IC_{50} than DTX-NLCs at all time points when treated with BTNW911 cells. Moreover, cell proliferation was reduced with increasing incubation time for all treatments, indicating a time-dependent cytotoxicity (Fig. S3a–c). ALA-DTX-NLCs displayed high efficacy when tested against 3D tumour spheroids with no significant difference in toxicity when compared to DTX, indicating that the formulation was as effective as the DTX alone. On the other hand, the GLA-DTX-NLCs demonstrated significant high IC_{50} value which indicated less toxicity when tested under similar conditions (Table 2). The tumour spheroids morphology in response to the dose, have been shown in Fig. 5a.

3.3.5. Cell cycle analysis

The illustration of cell cycle phases is shown in Fig. 5b. The cell cycle distribution for DTX-NLCs, GLA-DTX-NLCs and ALA-DTX-NLCs followed the same pattern as the DTX cell arrest during the G2/M phase, which was significantly higher as compared to the control untreated cells and followed this pattern starting from high G2/M phase to lower DTX-NLCs > GLA-DTX-NLCs > DTX > ALA-DTX-NLCs (Fig. 5c). G2/M checkpoint ensures that cells do not enter mitosis phase, resulting in death which in turn indicated its potent anticancer effect.

3.3.6. Seahorse test for the evaluation of DTX and DTX-NLCs

The cells were tested for its mitochondrial respiration function by measuring mitochondrial oxygen consumption rate (OCR) for mitochondrial activity and oxygen consumption. The surface functionalised formulations had a profound effect on OCR on cellular respiration (Fig. 5d). Further examination of the process-specific oxygen consumption indicated a higher effect of ALA-DTX-NLCs compared to the control of untreated cells and GLA-DTX-NLCs (Fig. S4a–e).

4. Discussion

Surgery, chemotherapy, radiotherapy, and immunotherapy are used for GB treatment. However, GB is still an incurable disease, and the current approved therapies have negligible impact on the mortality rate, and therefore new approaches are required for its successful treatment. In this study, the two PUFAs, GLA and ALA have been explored for surface functionalising of DTX-NLCs to improve its GB targeting and tumoricidal efficacy. Previous report from our group have unleashed the potential of NLCs with a tailored mix of liquid lipids to deliver CNS negative drug DTX across the 3D *in-vitro* BBB model without affecting the integrity of the barrier [7]. DTX-NLCs herein have been functionalised with two PUFAs to improve its tumoricidal effect and selective
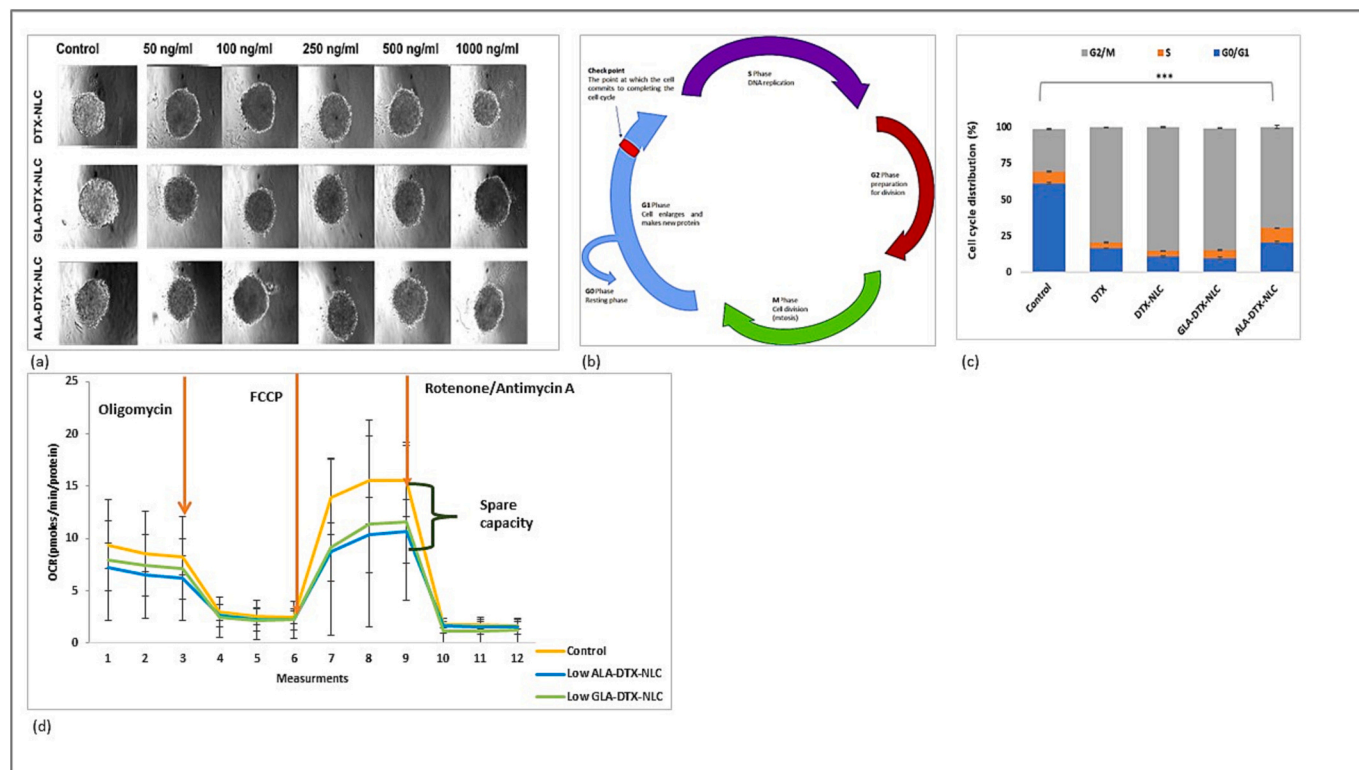
Fig. 5. (a) Tumour spheroids morphology (U87MG) following treatment with DTX-NLCs, GLA-DTX-NLCs, and ALA-DTX-NLCs (b) Illustration of cell cycle distribution, (c) Percentage cell cycle distribution for U87MG cell lines following 24 h incubation with various treatments, when formulations were compared to untreated U87MG as the control, (d) Mitochondrial activity and oxygen consumptions, U87MG cells were treated and incubated for 24 h with GLA-DTX-NLCs and ALA-DTX-NLCs. The control, in this case, is the non-treated cells. *** p < 0.000, refers to a very significant difference. Data are mean and ±SD, (*N*=3).

uptake towards GB cells. Since GLA and ALA are prone to oxidation, it was essential to maintain the ligands conjugation under controlled conditions. It has been reported that antioxidants especially Vit E might block the tumoricidal effect of the PUFAs (GLA/ALA) as it functions as a lipid peroxidase inhibitor and consequently decrease the inhibitory effect of the PUFAs *in-vitro* [37,39]. Therefore, the synthesis method of functionalisation of NLCs was carried out under nitrogen gas exposure to protect the PUFAs from degradation. The modification with GLA/ALA was achieved through forming amide linkage by a covalently coupling free amino group of DTX-NLCs to the carboxylic acid group present in GLA/ALA, using coupling agents EDC/NHS [40].

The developed DTX-NLCs were characterised with a high negative charge. Following the functionalisation of DTX-NLC surface with either GLA or ALA led to the ligands masking the surface charge causing reduction of the zeta potential [41]. Though high ligand density is desirable as high ligand concentration may lead to efficient binding to the target due to high avidity [42], but not at the cost of very high particle size as that would likely lead to opsonisation of the particles. Additionally, an earlier study by Elias et al. indicated that high ligand density does not always mean high binding to cells [42]. While both the ratios of FAG: GLA (1:1/5 and 1:1/6) displayed similar particle size, FAG: GLA (1:1/5) showed better activity in terms of inhibition of cell growth and was thus selected. Similarly, FAG: ALA of 1:1/6 showed favourable particle size and better anti-proliferative activity. The particle size of both selected surface modified NLCs was <160 nm, which might be useful for treating cancer since previously reported data indicated that small size particles tend to accumulate in the tumour tissues by virtue of enhanced permeation and retention (EPR) and the BBB passage of nanoparticles is critically affected by particle size apart from other factors [43–46].

Conjugation of GLA and ALA on to DTX-NLCs was also confirmed by FTIR spectra which revealed new peak formations and interaction due to peak shifting. Additionally, the drug release from the ligand appended GLA-DTX-NLCs and ALA-DTX-NLCs was slower than that of free-surface DTX-NLCs. This is in confirmation with previous reports where slower and prolonged release from ligand appended nanoparticles has been reported [30]. A sustained release is rather an attractive approach for anticancer drug delivery especially by intravenous route as it allows maintenance of steady concentrations of anticancer drug in the body for longer time intervals [47–49]. Slightly higher particle size of GLA-DTX-NLCs and ALA-DTX-NLCs in comparison to that of the bare DTX-NLCs and increase in gap between the drug containing core and surface of nanoparticles could be responsible for the sustained release [30,31].

The surface modified NLCs were evaluated *in-vitro* for their permeation through BBB and BBTB models. BBB and BBTB are major hurdles for chemotherapeutic drugs to overcome for brain tumour delivery. GLA-DTX-NLCs and ALA-DTX-NLCs showed two-fold higher penetration across BBB as compared to DTX-NLCs. Apart from benefiting from transient and reversible opening of TJs [50], which facilitated barrier penetration *via* paracellular transport [51], the surface modified NLCs utilised additional mechanism for their enhanced transport. The incorporation of Kolliphor®HS15 (a PEG copolymer/surfactant) in DTX-NLCs is reported to affect F-actin morphology regulating paracellular tightness and transport [52]. Furthermore, it works as an efflux pump P-gp inhibitor to reverse the multidrug resistance [53]. Moreover incorporation of soyalecithin and Phospholecithin H90 as surfactants has shown to facilitate transport of drugs to the brain [54,55]. GLA on the surface of the NLCs binds to the brain FABP7 receptors [56,57]. Also, fatty acids have the ability to enter the brain by passive diffusion and proteins-mediated transport by the membrane-associated proteins, like fatty acid transport proteins and fatty acid translocases (CD36) as indicated by Chen et al. [58]. Moreover, upon administration of GLA reactive oxygen species (ROS) are generated [59], that lead to the suppression of P-gp expression and eventually to P-gp inhibition [60], which in turn cause efflux pump inhibition and that explains the high fluorescence level of R-GLA-DTX-NLCs that was noted even following the closure of

TJs after transient opening. Both PUFA surface-modified formulations enhanced the permeation of R-DTX-NLCs. From this data, we can establish, that the mechanism for BBB permeability and uptake of NPs was thought to be receptor-mediated endocytosis by the brain capillary endothelial cells, followed by transcytosis [61]. Evidently, *in-vivo* GB is known to grow behind intact BBB, as well as causing a leaky BBB in the nearby vessels and the endothelial cells [29,62], resulting in enhanced permeation. In our study, the increase in paracellular permeability led to the excess NLCs permeating through the BBTB model in the presence of the GBs cells, suggesting the existence of GB cells promote endothelial permeability in brain microvascular endothelial cells as previously demonstrated by Dwyer et al. [63], in addition to other mechanism promoting permeation of R-GLA-DTX-NLCs and R-ALA-DTX-NLCs, through binding to the brain FABP7 receptors [56,57]. Overall, GLA and ALA appended NLCs can be considered highly permeable through BBB and BBTB *in-vitro* models, since the Papp values were higher than $>60 \times 10^{-6}$ cm/min.

DTX-NLCs and PUFA functionalised formulations were internalised into the cells through endocytosis process, with clathrin and macropinocytosis being the main pathways since uptake was reduced when the cells were incubated under hypertonic environment, and disruption of actin filament by cytochalasin B reduced the cell internalisation thus supporting involvement of these two pathways [64]. Higher cell uptake of PUFA appended formulations as compared to bare DTX-NLCs by GB cells reveal additional involvement of FABP or FABP7 for intracellular transport as they are highly upregulated in GBs cells in comparison with normal brain cells [22,23]. PUFAs have a limited effect on normal cells and high cytotoxicity towards cancerous cell lines [20], which are in line with our finding showing increased uptake by GB cells as compared normal SVG P12 brain cells. Our investigation showed that appending GLA/ALA significantly improved toxicity of the DTX-NLCs towards GBs cells probably due to higher cell uptake afforded by these formulations. The difference in IC$_{50}$ values was more evident at early time points of 24 and 48 h due active interalisation by receptor mediated endocytosis of functionalised NLCs. Previous literature has reported tumoricidal effect of GLA towards GBs cells however, *in vivo*, only intra-tumoral injection showed tumour regression as oral or intravenous administration failed to deliver GLA to tumour cells requiring better delivery methods [14,17,37,65]. In this context, use of GLA as ligand on a lipid nanoparticle for enhanced GB uptake and improved efficacy of chemotherapeutic drug is a novel approach to reap the benefits of this safe and well-established fatty acid. We hypothesize that the presence of GLA and ALA ligands on the DTX-NLCs would effectively inhibit the P-gp, thereby enhancing the chemotherapeutic efficacy of DTX. Higher activity of ALA-DTX-NLCs (13.9 fold at 24 h) towards patient derived BTNW911 cells further confirm the promise of these formulations in tumour that are resistant to chemotherapy. This is in line with previous study that has reported that PUFAs result in increased sensitivity to chemotherapy, especially in tumour lines that are resistant to chemotherapy, and cause higher cytotoxicity to a tumour [20]. Interestingly, our data showed ALA conjugated with the DTX-NLCs had similar efficacy as DTX when evaluated in 3D tumour spheroids. Since the cells on the surface of spheroids are likely to be killed quicker than the cells deeper in the spheroid [66], longer incubation time with the treatments might be favourable, as different formulations are exhibiting a variable reaction when incubated with the spheroids due to drug taking a longer time to penetrate the spheroid, depending on size, lipophilicity and surface modification [67]. Previous study showed doxorubicin a well-known anticancer drug was limited to the periphery of the spheroids and could not diffuse through the spheroid more than the outer few cell layers [68]. DTX transportation to the spheroid core has also shown to be challenging, as previously demonstrated by Gao et al. [66]. The direct contact of DTX with the spheroids might harm the cells and cause cell death, which makes the transportation of DTX from the surface of dead cells to the core of tumour spheroid impossible [69]. Therefore, the proposed encapsulation of DTX within the NLCs was a successful

approach to achieve high penetration and similar potency. The cell death was considered to be through the G2/M phase and causing cell arrest through breaking the double-strain DNA, and damaging of the chromosome [70]. A significant effect of GLA-DTX-NLCs and ALA-DTX-NLCs was observed on mitochondrial respiration as compared to non-treated cells. This suggests both formulations have a mitochondrial-specific effect, which is still unknown. It may be explained by the early-stage initiation of the apoptotic process and certainly requires more work to investigate the temporal and mechanical aspects of this observation. Moreover, both formulations caused a decrease in the mitochondrial reserve capacity of cells, indicating that the lipid carrier increased the drug's ability to impair oxygen consumption and thus the cells' ATP-producing capability [71].

5. Conclusion

To best of our knowledge in this present study both GLA-DTX-NLCs and ALA-DTX-NLCs are novel newly developed functionalised NLCs for brain-targeted therapy to treat GB, and no previous reports have demonstrated for the permeation of these ligand appended NLCs through a 3D BBB/BTB *in-vitro* barriers. We achieved a successful functionalisation of DTX-NLCs with two PUFAs (GLA and ALA) using EDC-NHS chemistry. GLA-DTX-NLCs and ALA-DTX-NLCs, exhibited a small and relatively uniform particle size distribution with high drug entrapment efficiency. FTIR spectral analysis, in addition to a reduction of zeta potential and free surface amines, confirmed the covalent bonding of ligands to the NLC formulation. We have shown a distinctive increase in the apparent permeability and high fluorescence concentration permeation through the *in-vitro* BBTB model in the presence of GB cells with successful uptake by GB, as compared to bare DTX-NLCs which acclaims not only their enhanced BBB permeability but also, improved cellular internalisation and selective uptake. Furthermore, the fluorescence microscopy and FACS analysis also confirmed the preferential uptake of NLCs by GB cells as compared to normal cells when the DTX-NLCs were surface modified with GLA and ALA with high efficacy and improved DTX toxicity towards GB cells. Though both PUFAs have shown promise, ALA-DTX-NLCs were more effective, which merits their potential in cancer therapy that would contribute to the ongoing research for the treatment of a brain tumour, primarily for GB targeted therapy.

Author agreement

All authors can certify that they have seen and approved the final version of the manuscript being submitted, and it is original work, that hasn't received prior publication and isn't under consideration for publication elsewhere.

Funding source declaration

All authors can declare that no funding or research grants (and their source) received in the course of study, research or assembly of the manuscript.

Declaration of competing interest

The authors declare that they have no known competing financial interests or personal relationships that could have appeared to influence the work reported in this paper.

Data availability

Data will be made available on request.

Acknowledgement

Appendix A. Supplementary data

Supplementary data to this article can be found online at https://doi.org/10.1016/j.bioadv.2023.213660.

References

[1] T.R. Alves, F.R.S. Lima, S.A. Kahn, D. Lobo, L.G.F. Dubois, R. Soletti, et al., Glioblastoma cells: a heterogeneous and fatal tumor interacting with the parenchyma, Life Sci. (2011) 532–539.

[2] H. Xin, X. Sha, X. Jiang, W. Zhang, L. Chen, X. Fang, Anti-glioblastoma efficacy and safety of paclitaxel-loading Angiopep-conjugated dual targeting PEG-PCL nanoparticles, Biomaterials. 33 (32) (2012).

[3] M. Masserini, Nanoparticles for brain drug delivery, ISRN Biochem. 21 (2013) (2013 May) 1–18.

[4] N.J.S. Fauzee, Taxanes: promising anti-cancer drugs, Asian Pac J Cancer Prev [Internet]. 12 (4) (2011) 837–851. Available from: http://www.ncbi.nlm.nih.gov/pubmed/21790213.

[5] W. Löscher, H. Potschka, Role of drug efflux transporters in the brain for drug disposition and treatment of brain diseases, Prog. Neurobiol. 76 (1) (2005) 22–76.

[6] D. Wang, C. Wang, L. Wang, Y. Chen, A comprehensive review in improving delivery of small-molecule chemotherapeutic agents overcoming the blood-brain/brain tumor barriers for glioblastoma treatment, Drug Deliv [Internet]. 26 (1) (2019 Jan 1) 551–565. Available from: https://www.tandfonline.com/doi/full/10.1080/10717544.2019.1616235.

[7] T. Zwain, J. Elizabeth, B. Sabagh, A. Shaw, A.J. Burrow, K.K. Singh, Materials Science & Engineering C Tailoring functional nanostructured lipid carriers for glioblastoma treatment with enhanced permeability through in-vitro 3D BBB / BBTB models, Materials Science & Engineering C [Internet] 121 (October 2020) (2021), 111774. Available from: https://doi.org/10.1016/j.msec.2020.111774.

[8] R.H. Müller, M. Radtke, S.A. Wissing, Solid lipid nanoparticles (SLN) and nanostructured lipid carriers (NLC) in cosmetic and dermatological preparations, Adv Drug Deliv Rev [Internet]. 54 (2002 Nov) S131–S155. Available from: https://linkinghub.elsevier.com/retrieve/pii/S0169409X02001187.

[9] J. Garg, K. Pathania, S.P. Sah, S.V. Pawar, Nanostructured lipid carriers: a promising drug carrier for targeting brain tumours. Futur, J. Pharm. Sci. 8 (1) (2022 Dec).

[10] A. Michalak, P. Mosińska, J. Fichna, Polyunsaturated Fatty Acids and their Derivatives: Therapeutic Value for Inflammatory, Functional Gastrointestinal Disorders, and Colorectal cancer vol. 7, Frontiers Media S.A., 2016. Frontiers in Pharmacology.

[11] H.A. Leaver, S.B. Wharton, H.S. Bell, I.M.M. Leaver-Yap, I.R. Whittle, Highly unsaturated fatty acid induced tumour regression in glioma pharmacodynamics and bioavailability of gamma linolenic acid in an implantation glioma model: effects on tumour biomass, apoptosis and neuronal tissue histology, Prostaglandins Leukot. Essent. Fatty Acids 67 (5) (2002).

[12] U.N. Das, Essential fatty acids, lipid peroxidation and apoptosis, Prostaglandins Leukot. Essent. Fatty Acids 61 (3) (1999).

[13] H.S. Bell, S.B. Wharton, H.A. Leaver, I.R. Whittle, Effects of N-6 essential fatty acids on glioma invasion and growth: experimental studies with glioma spheroids in collagen gels, J. Neurosurg. 91 (6) (1999).

[14] J.A. Miyake, Gamma-linolenic acid inhibits both tumour cell cycle progression and angiogenesis in the orthotopic C6 glioma model through changes in VEGF, Flt1, ERK1/2, MMP2, cyclin D1, pRb, p53 and p27 protein expression, Lipids Health Dis. 8 (2009).

[15] M.F. Cury-Boaventura, C. Pompéia, R. Curi, Comparative toxicity of oleic acid and linoleic acid on Raji cells, Nutrition. 21 (3) (2005).

[16] T.Y. Chi, G.G. Chen, P.B.S. Lai, Eicosapentaenoic acid induces fas-mediated apoptosis through a p53-dependent pathway in hepatoma cells, Cancer J. 10 (3) (2004).

[17] U.N. Das, γ-Linolenic acid therapy of human glioma - a review of in vitro, in vivo, and clinical studies, Med. Sci. Monit. 13 (7) (2007). RA119-31.

[18] M. Jóźwiak, A. Filipowska, F. Fiorino, M. Struga, Anticancer activities of fatty acids and their heterocyclic derivatives, Eur. J. Pharmacol. 871 (2020), 172937.

[19] Huan M. Lei, Zhou S. Yuan, Teng Z. Hui, Zhang B. Le, Liu X. You, Wang J. Pin, et al., Conjugation with α-linolenic acid improves cancer cell uptake and cytotoxicity of doxorubicin, Bioorg. Med. Chem. Lett. 19 (9) (2009) 2579–2584.

[20] E. Horia, B.A. Watkins, Comparison of stearidonic acid and α-linolenic acid on PGE 2 production and COX-2 protein levels in MDA-MB-231 breast cancer cell cultures, J. Nutr. Biochem. 16 (3) (2005).

[21] B.M. Forman, J. Chen, R.M. Evans, Hypolipidemic drugs, polyunsaturated fatty acids, and eicosanoids are ligands for peroxisome proliferator-activated receptors α and δ, Proc. Natl. Acad. Sci. U. S. A. 94 (9) (1997).

[22] R. Mita, J.E. Coles, D.D. Glubrecht, R. Sung, X. Sun, R. Godbout, B-FABP-expressing radial glial cells: the malignant glioma cell of origin? Neoplasia. 9 (7) (2007).

[23] Y. Liang, M. Diehn, N. Watson, A.W. Bollen, K.D. Aldape, M.K. Nicholas, et al., Gene expression profiling reveals molecularly and clinically distinct subtypes of glioblastoma multiforme, Proc. Natl. Acad. Sci. U. S. A. 102 (16) (2005).

[24] G. Sanità, B. Carrese, A. Lamberti, Nanoparticle surface functionalization: how to improve biocompatibility and cellular internalization, Frontiers in Molecular Biosciences 7 (2020).

[25] R.W. Mitchell, N.H. On, M.R. Del Bigio, D.W. Miller, G.M. Hatch, Fatty acid transport protein expression in human brain and potential role in fatty acid transport across human brain microvessel endothelial cells, J. Neurochem. 117 (4) (2011).

[26] B. Gabold, F. Adams, S. Brameyer, K. Jung, C.L. Ried, T. Merdan, et al., Transferrin-modified chitosan nanoparticles for targeted nose-to-brain delivery of proteins, Drug Deliv. Transl. Res. 13 (3) (2023 Mar 1) 822–838.

[27] Y. Gao, W. Sun, J. Zhang, Optimization of preparation and property studies on glycosylated albumin as drug carrier for nanoparticles, Pharmazie. 66 (7) (2011).

[28] C.L. Esposito, S. Nuzzo, S.A. Kumar, A. Rienzo, C.L. Lawrence, R. Pallini, et al., A combined microRNA-based targeted therapeutic approach to eradicate glioblastoma stem-like cells, Journal of Controlled Release [Internet]. 238 (2016 Sep) 43–57. Available from: https://linkinghub.elsevier.com/retrieve/pii/S0168365916304667.

[29] S. Kumar, L. Shaw, C. Lawrence, R. Lea, J. Alder, P50 * developing a physiologically relevant blood brain barrier model for the study of drug disposition in glioma, Neuro Oncol [Internet]. 16 (Suppl. 6) (2014 Oct 1) vi8–vi8. Available from: https://academic.oup.com/neuro-oncology/article-lookup/doi/10.1093/neuonc/nou249.38.

[30] M.N. Koopaei, M.R. Khoshayand, S.H. Mostafavi, M. Amini, M.R. Khorramizadeh, M.J. Tehrani, et al., Docetaxel loaded PEG-PLGA nanoparticles: optimized drug loading, in-vitro cytotoxicity and in-vivo antitumor effect, Iranian Journal of Pharmaceutical Research. 13 (3) (2014) 819–833.

[31] Z. Xu, L. Chen, W. Gu, Y. Gao, L. Lin, Z. Zhang, et al., The performance of docetaxel-loaded solid lipid nanoparticles targeted to hepatocellular carcinoma, Biomaterials. 30 (2) (2009).

[32] I. Singh, R. Swami, M.K. Jeengar, W. Khan, R. Sistla, P-Aminophenyl-α-d-mannopyranoside engineered lipidic nanoparticles for effective delivery of docetaxel to brain, Chem. Phys. Lipids 188 (2015) 1–9.

[33] W. Tao, X. Zeng, T. Liu, Z. Wang, Q. Xiong, C. Ouyang, et al., Docetaxel-loaded nanoparticles based on star-shaped mannitol-core PLGA-TPGS diblock copolymer for breast cancer therapy, Acta Biomater. 9 (11) (2013) 8910–8920.

[34] C. Houacine, D. Adams, K.K. Singh, Impact of liquid lipid on development and stability of trimyristin nanostructured lipid carriers for oral delivery of resveratrol, J. Mol. Liq. 9 (12) (2020), 1852.

[35] T. Lin, P. Zhao, Y. Jiang, Y. Tang, H. Jin, Z. Pan, et al., Blood-brain-barrier-penetrating albumin nanoparticles for biomimetic drug delivery via albumin-binding protein pathways for antiglioma therapy, ACS Nano 10 (11) (2016).

[36] G.L. Amidon, H. Lennernäs, V.P. Shah, J.R. Crison, A theoretical basis for a biopharmaceutic drug classification: the correlation of in vitro drug product dissolution and in vivo bioavailability, Pharmaceutical Research: An Official Journal of the American Association of Pharmaceutical Scientists. 12 (3) (1995).

[37] U.N. Das, From bench to the clinic: -linolenic acid therapy of human gliomas, Prostaglandins Leukotrienes and Essential Fatty Acids. 70 (2004).

[38] N.K.Y. Wong, R.A. Shenoi, S. Abbina, I. Chafeeva, J.N. Kizhakkedathu, M.K. Khan, Nontransformed and cancer cells can utilize different endocytic pathways to internalize dendritic nanoparticle variants: implications on nanocarrier design, Biomacromolecules. 18 (8) (2017) 2427–2438.

[39] J.A. Menéndez, Barbacid M. Del Mar, S. Montero, E. Sevilla, E. Escrich, M. Solanas, et al., Effects of gamma-linolenic acid and oleic acid on paclitaxel cytotoxicity in human breast cancer cells, Eur. J. Cancer 37 (3) (2001).

[40] Q. Zhang, R.X. Li, X. Chen, X.X. He, A.L. Han, G.Z. Fang, et al., Study of efficiency of coupling peptides with gold nanoparticles, Chin. J. Anal. Chem. 45 (5) (2017).

[41] Y. Han, Y. Zhang, D. Li, Y. Chen, J. Sun, F. Kong, Transferrin-modified nanostructured lipid carriers as multifunctional nanomedicine for codelivery of DNA and doxorubicin, Int. J. Nanomedicine 9 (2014) 4107–4116.

[42] D.R. Elias, A. Poloukhtine, V. Popik, A. Tsourkas, Effect of ligand density, receptor density, and nanoparticle size on cell targeting, Nanomedicine. 9 (2) (2013).

[43] Y. Zhou, Z. Peng, E.S. Seven, R.M. Leblanc, Crossing the blood-brain barrier with nanoparticles, J. Control. Release 270 (2018).

[44] M. Patel, E.B. Souto, K.K. Singh, Advances in brain drug targeting and delivery: limitations and challenges of solid lipid nanoparticles, Expert Opin. Drug Deliv. 10 (7) (2013) 889–905.

[45] J.Y. Choi, T. Ramasamy, T.H. Tran, S.K. Ku, B.S. Shin, H.G. Choi, et al., Systemic delivery of axitinib with nanohybrid liposomal nanoparticles inhibits hypoxic tumor growth, J. Mater. Chem. B 3 (2015) 408–416.

[46] M. Nowak, T.D. Brown, A. Graham, M.E. Helgeson, S. Mitragotri, Size, shape, and flexibility influence nanoparticle transport across brain endothelium under flow, Bioeng Transl Med. 5 (2) (2020).

[47] P. Mathur, S. Sharma, S. Rawal, B. Patel, M.M. Patel, Fabrication, optimization, and in vitro evaluation of docetaxel-loaded nanostructured lipid carriers for improved anticancer activity, J. Liposome Res. 30 (2) (2020).

[48] J. Varshosaz, M.A. Davoudi, S. Rasoul-Amini, Docetaxel-loaded nanostructured lipid carriers functionalized with trastuzumab (Herceptin) for HER2-positive breast cancer cells, J. Liposome Res. 28 (4) (2018).

[49] D. Liu, Z. Liu, L. Wang, C. Zhang, N. Zhang, Nanostructured lipid carriers as novel carrier for parenteral delivery of docetaxel, Colloids Surf. B Biointerfaces 85 (2) (2011) 262–269.

[50] G. Bazzoni, Endothelial tight junctions: permeable barriers of the vessel wall, Thromb. Haemost. 95 (1) (2006).

[51] B. Singh, Crossing Blood-Brain Barrier Using Drug Delivery: A Successful Venture Using Lipidic Nanostructured Systems, Available from: https://www.researchgate.net/publication/247160958, 2014.

[52] S. Shubber, D. Vllasaliu, C. Rauch, F. Jordan, L. Illum, S. Stolnik, Mechanism of mucosal permeability enhancement of CriticalSorb® (Solutol® HS15) investigated in vitro in cell cultures, Pharm. Res. 32 (2) (2015 Feb 5) 516–527. Available from: http://link.springer.com/10.1007/s11095-014-1481-5.

[53] J.S. Coon, W. Knudson, K. Clodfelter, B. Lu, R.S. Weinstein, Solutol HS 15, nontoxic polyoxyethylene esters of 12-hydroxystearic acid, reverses multidrug resistance, Cancer Res [Internet]. 51 (3) (1991 Feb 1) 897–902. Available from: http://www.ncbi.nlm.nih.gov/pubmed/1988130.

[54] P. Girotra, S.K. Singh, Multivariate optimization of rizatriptan benzoate-loaded solid lipid nanoparticles for brain targeting and migraine management, AAPS PharmSciTech 18 (2) (2017).

[55] P. Blasi, S. Giovagnoli, A. Schoubben, M. Ricci, C. Rossi, Solid lipid nanoparticles for targeted brain drug delivery☆, Adv Drug Deliv Rev [Internet]. 59 (6) (2007 Jul 10) 454–477. Available from: https://linkinghub.elsevier.com/retrieve/pii/S0169409X07000427.

[56] F. Shimizu, T.K. Watanabe, H. Shinomiya, Y. Nakamura, T. Fujiwara, Isolation and expression of a cDNA for human brain fatty acid-binding protein (B-FABP), Biochim. Biophys. Acta Gene Struct. Expr. 1354 (1) (1997).

[57] M.E. Elsherbiny, M. Emara, R. Godbout, Interaction of brain fatty acid-binding protein with the polyunsaturated fatty acid environment as a potential determinant of poor prognosis in malignant glioma, Prog. Lipid Res. 52 (4) (2013) 562–570.

[58] C.T. Chen, J.T. Green, S.K. Orr, R.P. Bazinet, Regulation of brain polyunsaturated fatty acid uptake and turnover, Prostaglandins Leukot. Essent. Fatty Acids 79 (3–5) (2008).

[59] H.A. Leaver, H.S. Bell, M.T. Rizzo, J.W. Ironside, A. Gregor, S.B. Wharton, et al., Antitumour and pro-apoptotic actions of highly unsaturated fatty acids in glioma, Prostaglandins Leukot. Essent. Fatty Acids 66 (1) (2002).

[60] H. Yuan, J. Miao, Y.Z. Du, J. You, F.Q. Hu, S. Zeng, Cellular uptake of solid lipid nanoparticles and cytotoxicity of encapsulated paclitaxel in A549 cancer cells, Int. J. Pharm. 348 (1–2) (2008).

[61] R. Gabathuler, Approaches to transport therapeutic drugs across the blood-brain barrier to treat brain diseases, Neurobiol. Dis. 37 (2010).

[62] N.H. On, R. Mitchell, S.D. Savant, C.J. Bachmeier, G.M. Hatch, D.W. Miller, Examination of blood-brain barrier (BBB) integrity in a mouse brain tumor model, J. Neurooncol 111 (2) (2013).

[63] J. Dwyer, J.K. Hebda, A. Le Guelte, E.M. Galan-Moya, S.S. Smith, S. Azzi, et al., Glioblastoma cell-secreted Interleukin-8 induces brain endothelial cell permeability via CXCR2, PloS 7 (9) (2012), e45562.

[64] S. Martins, S. Costa-Lima, T. Carneiro, A. Cordeiro-Da-Silva, E.B. Souto, D.C. Ferreira, Solid lipid nanoparticles as intracellular drug transporters: an investigation of the uptake mechanism and pathway, Int. J. Pharm. 430 (1–2) (2012).

[65] A. Bakshi, D. Mukherjee, A. Bakshi, A.K. Banerji, U.N. Das, γ-Linolenic acid therapy of human gliomas, Nutrition. 19 (4) (2003).

[66] H. Gao, S. Zhang, Z. Yang, S. Cao, X. Jiang, Z. Pang, In vitro and in vivo intracellular distribution and anti-glioblastoma effects of docetaxel-loaded nanoparticles functioned with IL-13 peptide, Int. J. Pharm. 466 (1–2) (2014).

[67] A. Tchoryk, V. Taresco, R.H. Argent, M. Ashford, P.R. Gellert, S. Stolnik, et al., Penetration and uptake of nanoparticles in 3D tumor spheroids, Bioconjug Chem [Internet]. 30 (5) (2019 May 15) 1371–1384. Available from: https://pubs.acs.org/doi/10.1021/acs.bioconjchem.9b00136.

[68] M. Wartenberg, H. Acker, Induction of cell death by doxorubicin in multicellular spheroids as studied by confocal laser scanning microscopy, Anticancer Res 16 (2) (1996).

[69] H. Gao, Z. Yang, S. Cao, Y. Xiong, S. Zhang, Z. Pang, et al., Tumor cells and neovasculature dual targeting delivery for glioblastoma treatment, Biomaterials. 35 (7) (2014).

[70] A.H. Ree, T. Stokke, Å. Bratland, S. Patzke, R.V. Nome, S. Folkvord, et al., DNA damage responses in cell cycle G2 phase and mitosis - tracking and targeting, Anticancer Res 26 (3 A) (2006).

[71] R. Wen, B. Banik, R.K. Pathak, A. Kumar, N. Kolishetti, S. Dhar, Nanotechnology inspired tools for mitochondrial dysfunction related diseases, Adv Drug Deliv Rev [Internet]. 99 (2016 Apr) 52–69. Available from: https://linkinghub.elsevier.com/retrieve/pii/S0169409X16300023.